The effects of third alloying elements on the bulk Ag$_3$Sn formation in slowly cooled Sn–3.5Ag lead-free solder

Jun Shen · Shiqiang Lai · Yongchang Liu ·
Houxiu Gao · Jun Wei

Abstract The effects of third alloying elements (Cu, In, Zn) on the formation of bulk Ag$_3$Sn intermetallic compounds (IMCs) in slowly cooled Sn–3.5Ag lead-free solder were investigated by microstructural observation and thermal analysis technique. Microstructural observation shows that bulk Ag$_3$Sn IMCs existed in the microstructure of slowly cooled Sn–3.5Ag, Sn–3.5Ag–0.75Cu and Sn–3.5Ag–1.5In alloys, while no bulk Ag$_3$Sn IMCs formed in the slowly cooled Sn–3.5Ag–2.0Zn alloys. Thermal analysis results indicate that Ag preferably reacted with Zn to form Ag–Zn IMCs at high temperature rather than reacted with Sn to form Ag$_3$Sn plate.

1 Introduction

Sn–Ag alloy has been identified as Pb-free solder candidate to replace Pb-bearing solders in microelectronic applications [1]. However, recent investigations on the processing behavior and solder joints reliability assessment have revealed several potential reliability risk factors associated with this alloy. The formation of bulk Ag$_3$Sn plates in Sn–Ag alloy joints, especially when solidified in a relatively slow cooling rate, is one issue of the concern [2, 3]. The required undercooling degree of β-Sn is larger than that of Ag$_3$Sn phase in this solder, therefore the Ag$_3$Sn crystal nucleus should form at the onset of eutectic reaction [4, 5]. The nucleated Ag$_3$Sn phase could become an epitaxial sink for Ag and Sn atoms, leading to the growth of the Ag$_3$Sn crystal in a plate-like morphology [6]. This excessive growth of Ag$_3$Sn in Sn–Ag lead-free solder degrades the thermal fatigue life, plastic-deformation properties and tensile strength of the solder joints [2].

The formation of bulk Ag$_3$Sn plate can be kinetically suppressed by increasing the solidification rate of Sn–3.5Ag alloy. An increase in cooling rate will provide greater undercooling to induce nucleation of primary β-Sn crystal. β-Sn possesses a non-facet structure, while Ag$_3$Sn has a facet structure. When β-Sn phase acts as the primary phase, a higher driving force for the Ag$_3$Sn phase formation in an eutectic reaction and clinging around the primary β-Sn crystal is required due to the crystalline orientation mismatch between β-Sn and Ag$_3$Sn. Consequently, the Ag$_3$Sn particles have to nucleate more or less homogenously, and no bulk Ag$_3$Sn IMCs could separate out through the eutectic reaction [6, 7].

However, providing a high cooling rate is not always practical, especially in the case of large-thermal-mass chip carriers. Some researchers proposed one approach to avoid the formation of bulk Ag$_3$Sn plate by adding discrete secondary particles (such as rare earth elements or nanoparticles) into a solder matrix so as to form a composite solder [8, 9]. Since those secondary particles have been proved to be very effective surface-active reagents, they can significantly refine the size of Ag$_3$Sn IMCs during solder alloy solidification for the strong adsorption effect. But it is difficult to homogeneously distribute the secondary particles into composite solder.

J. Shen (✉) · S. Lai
College of Mechanical Engineering, Chongqing University, Chongqing 400044, PR China
e-mail: shenjun2626@163.com

Y. Liu · H. Gao
College of Materials Science & Engineering, Tianjin University, Tianjin 300072, PR China

J. Wei
Singapore Institute of Manufacturing Technology, 71 Nanyang Drive, Singapore 638075, Singapore

Another potentially viable and economically affordable approach to control the formation of bulk Ag₃Sn plate in Sn–Ag solder is adding minor third alloying elements. Kang et al. reported that Ag₃Sn plate formation can be controlled in near-ternary-eutectic Sn–Ag–Cu solder by minor Zn alloying. The minor Zn addition was found to be effective in reducing the amount of undercooling required for Sn solidification and thereby to suppress the formation of large Ag₃Sn plates [10].

To our knowledge, these studies only investigated the influence of Zn on the formation of bulk Ag₃Sn plate in Sn–Ag–Cu solder. Furthermore, the studies mainly focused on the decrease of undercooling required for Sn solidification and the relationship between the undercooling and the microstructure. However, the intrinsic mechanism for the decrease of undercooling, especially the solidification process of Sn–Ag alloy with/without another alloying element is still not clear.

In this paper, a thermal analysis technique was adopted to investigate the effects of third alloying elements on the formation of bulk Ag₃Sn in slowly cooled Sn–3.5Ag lead-free solder. The ternary alloys under study include Sn–3.5Ag–0.75Cu, Sn–3.5Ag–1.5In and Sn–3.5Ag–2.0Zn alloys (in mass%, hereafter). These alloys are usually used in industry system. The intrinsic mechanism of undercooling decrease and the relationship between the microstructure and solidification process in these alloys are discussed in details.

2 Experimental procedures

Sn–3.5Ag, Sn–3.5Ag–0.75Cu, Sn–3.5Ag–1.5In, and Sn–3.5Ag–2.0Zn alloys were prepared from bulk rods of pure Sn, Ag, Cu, In, and Zn. After weighing the individual pure metals, they were mixed and melted in a vacuum arc furnace under a high-purity argon atmosphere to produce button-like specimens with a diameter of about 3.5 cm. In order to get a homogeneous composition, all ingots were remelted five times. Finally they were solidified in a water-cooled copper mould with a cooling rate of about 20 K s⁻¹.

All solidified alloys were then cut into small specimen with a dimension of $\phi 5 \times 2$ mm, and a Netzsch DSC 404C apparatus was adopted for differential thermal analysis (DTA) measurements. The isochronal measurement DTA signals were calibrated and corrected by the Curie point of pure Fe and heat capacity of sapphire according to the method described in Ref. [11] This common method of heat capacity calibration in non-isothermal DTA is used to calculate the value of the apparent heat capacity of a sample ($C_{p,s}^{app}$) assuming that the measured temperature difference is proportional to the heat capacity of the specimen:

$$C_{p,s}^{app} = C_{p,cal} \frac{\Delta T_{t,s}}{\Delta T_{t,cal}}, \tag{1}$$

where $C_{p,cal}$ is the heat capacity of the calibration material (which equals the product of the number of moles of the calibration material and the literature value for the molar heat capacity of the calibration material), $\Delta T_{t,s}$ and $\Delta T_{t,cal}$ are the measurement signals from the DTA measurements on the calibration material and on the sample, respectively. Thus, determined value for the heat capacity is an apparent heat capacity because the influence of smearing over time is neglected.

DTA measurement was done under the protection of high-purity argon to avoid any unexpected oxidation. The applied thermal treatment procedure in the calorimetric experiment was as follows: the specimen was firstly heated up from room temperature up to 543 K with a constant rate of 5 K min⁻¹ and kept at this temperature for 10 min. Then it was cooled to room temperature (~300 K) with a rate of 5 K min⁻¹.

The microstructures of these specimens after DTA measurement were prepared by standard metallographic procedures. The specimens were mechanically polished with 1 μm diamond paste and etched with a solution of 5 vol.% HNO₃ + 95 vol.% C₂H₅OH. Scanning electron microscopy (FEI, Inc. XL30ESEM) was used for the observation of microstructures. Energy dispersive X-ray spectroscopy (OXFORD, Inc. ISIS300) and X-ray diffraction (Rigaku, Inc. D/max 2500v/pc) were used to determine the phase composition of the alloys.

3 Results

The microstructures of Sn–3.5Ag, Sn–3.5Ag–0.75Cu, Sn–3.5Ag–1.5In and Sn–3.5Ag–2.0Zn alloys are shown in Fig. 1. The X-ray diffraction spectra of the alloys are shown in Fig. 2. The compositions of various phases in the microstructure indicated by number are shown in Table 1. According to the microstructural observations, X-ray diffraction spectra and EDS analysis results, large bulk plate phases in Sn–3.5Ag, Sn–3.5Ag–0.75Cu and Sn–3.5Ag–1.5In alloys are Ag₃Sn, and the other phases in Sn–3.5Ag–0.75Cu, Sn–3.5Ag–1.5In and Sn–3.5Ag–2.0Zn alloys indicated by number are Cu₆Sn₅ phase, AgIn phase, and AgZn₃ phase, respectively.

Microstructural observation shows that bulk Ag₃Sn IMCs exists in the microstructure of slowly cooled Sn–3.5Ag, Sn–3.5Ag–0.75Cu, and Sn–3.5Ag–1.5In specimens, while no bulk Ag₃Sn IMCs formed in slowly cooled Sn–3.5Ag–2.0Zn specimen. Hence, only minor Zn addition can suppress the formation of large Ag₃Sn plates in Sn–3.5Ag alloy.

Fig. 1 Microstructure of slowly cooled (**a**) Sn–3.5Ag alloy, (**b**) Sn–3.5Ag–0.75Cu alloy, (**c**) Sn–3.5Ag–1.5In alloy, and (**d**) Sn–3.5Ag–2.0Zn alloy
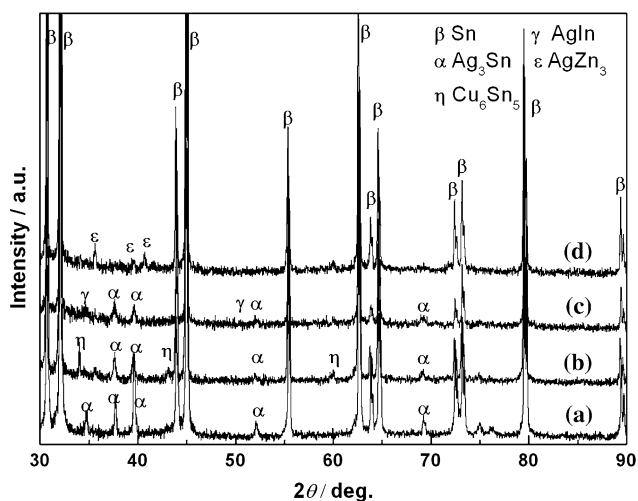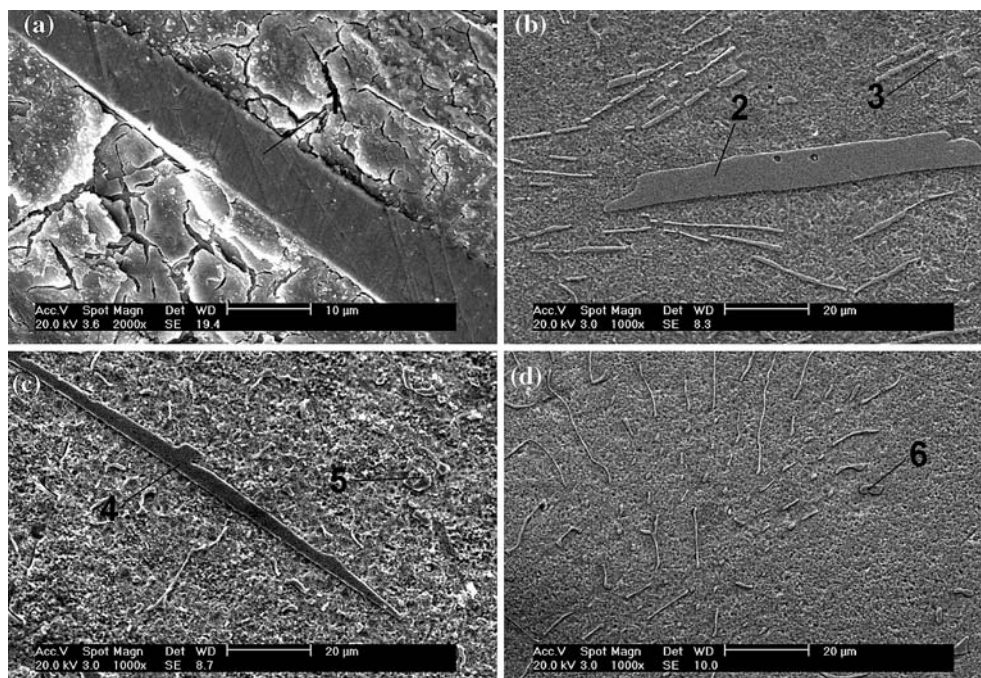

Fig. 2 The X-ray diffraction spectra of the slowly cooled (**a**) Sn–3.5Ag alloy, (**b**) Sn–3.5Ag–0.75Cu alloy, (**c**) Sn–3.5Ag–1.5In alloy, and (**d**) Sn–3.5Ag–2.0Zn alloy

Table 1 EDS results of the indicated typical regions in the investigated alloys

Solder alloys	Zone	Alloys composition/at.%		Phase identification
Sn–3.5Ag	1	Sn:40.49	Ag:41.91	Ag$_3$Sn
Sn–3.5Ag–0.75Cu	2	Sn:52.35	Ag:47.65	Ag$_3$Sn
	3	Sn:44.43	Cu:55.57	Cu$_6$Sn$_5$
Sn–3.5Ag–1.5In	4	Sn:50.55	Ag:49.45	Ag$_3$Sn
	5	Ag:77.81	In:22.19	AgIn
Sn–3.5Ag–2.0Zn	6	Ag:47.37	Zn:52.63	AgZn$_3$

As reported by Kang et al. [10] minor Zn addition was found to suppress the formation of large Ag$_3$Sn plates in Sn–Ag–Cu solder due to the effective reduction in the amount of undercooling required for Sn solidification. In order to verify this conclusion, DTA measurements were adopted to measure undercooling of Sn–3.5Ag, Sn–3.5Ag–0.75Cu, Sn–3.5Ag–1.5In, and Sn–3.5Ag–2.0Zn alloys. Figure 3 shows the apparent heat capacities of those four alloys measured with a heating/cooling rate of 5 K min^{-1}. Melt temperature point and solidification temperature point of these alloys can be obtained by those apparent heat capacity curves. The melt temperatures, solidification temperatures, and undercooling of alloys are listed in Table 2. It can be seen only the addition of a minor Zn into the Sn–3.5Ag alloy reduced the amount of undercooling required for alloy solidification significantly. According to the microstructural observation result, only a minor Zn addition into the Sn–3.5Ag alloy reduced the amount of undercooling significantly and suppressed the formation of large Ag$_3$Sn plates in it. Hence, suppressing the formation of large Ag$_3$Sn plates in Sn–3.5Ag alloy attributes to the undercooling degree decrease when Zn is added into this alloy.

4 Discussions

The experimental observation revealed the relationship between the undercooling decrease and the suppression effect of large Ag$_3$Sn plates. But the reason for the undercooling decrease when Zn was added into Sn–3.5Ag
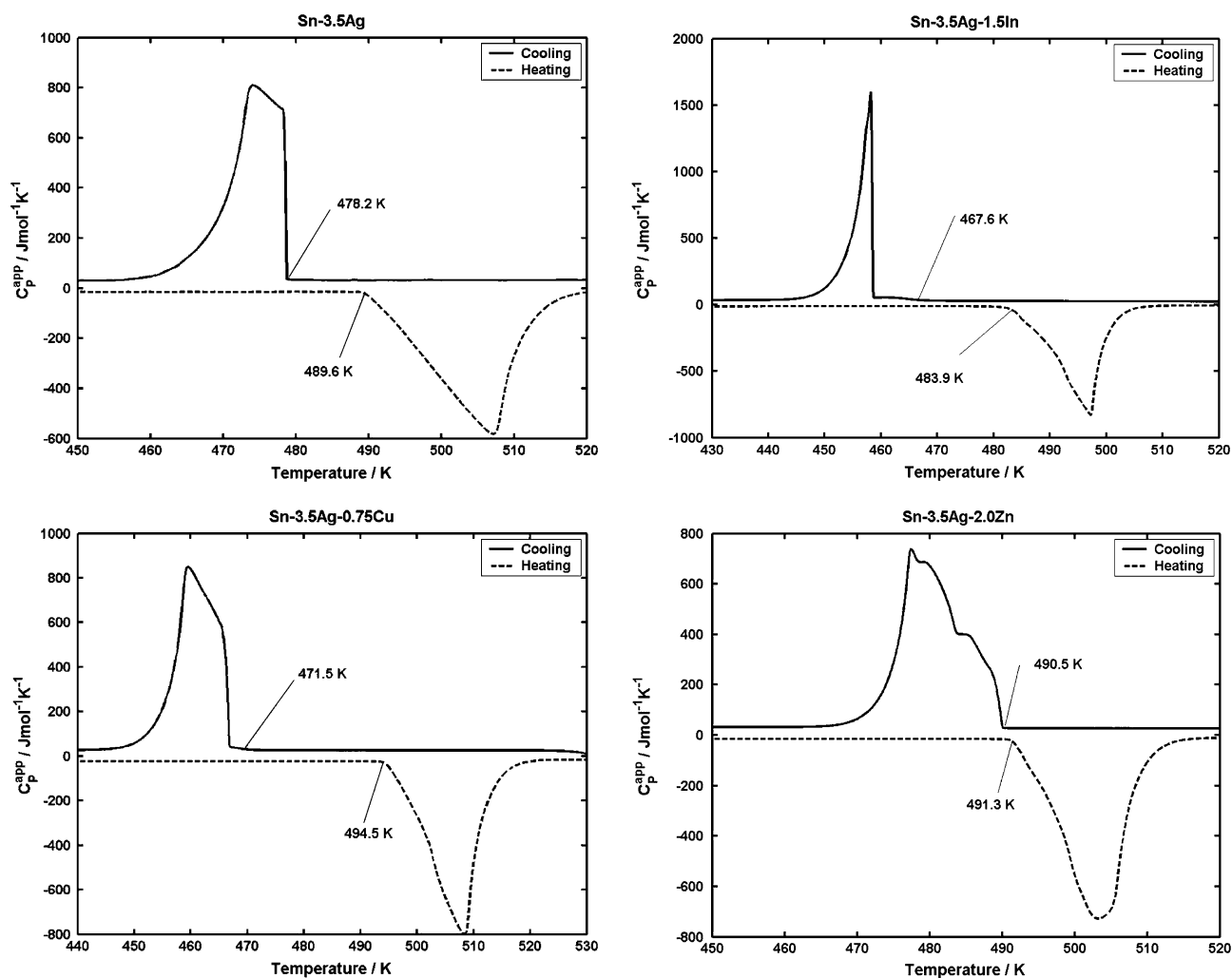
Fig. 3 Apparent heat capacity of alloys measured with a heating/cooling rate of 5 K min^{-1}

Table 2 Composition, melt/solidification temperatures and undercooling of alloys

Alloy composition	Solidification temperature T_1/K	Melt temperature T_2/K	Undercooling $\Delta T(=T_1 - T_2)$/K
Sn–3.5Ag	478.2	489.6	11.4
Sn–3.5Ag–0.75Cu	471.5	494.5	23.0
Sn–3.5Ag–1.5In	467.6	483.9	16.3
Sn–3.5Ag–2.0Zn	490.5	491.3	0.8

alloy needs further investigation. Hence, a general procedure for the determination of transformation rate of solid phase fractions into the solidified alloys from the recorded apparent heat capacity curve, which was firstly developed by Kempen et al., was adopted to determine the solidification process of the alloys [12].

The liquid fraction, f_l, and the enthalpy difference between the liquid and solid ΔH_{sl}, have been determined as a function of temperature in the measured curves of apparent heat capacity. The apparent heat capacity, $C_{p,m}$, includes the heat of transformation and the change in the heat

capacity of liquid, $C_{p,l}$, and of solid, $C_{p,s}$, induced by temperature change:

$$C_{p,m}(T) = f_l C_{p,l}(T) + f_s C_{p,s}(T) + \frac{\mathrm{d}f_s}{\mathrm{d}T}\Delta H_{sl}(T), \qquad (2)$$

where the solid fraction, f_s, equals $1 - f_l$. The first two terms at the right-hand side of the above equation state that the heat capacity of both liquid and solid phases can be given as the weighted (according to the amounts of the individual phases) average of the heat capacities of the individual phases. The last term at the right-hand side

represents the (reaction) enthalpy released during solidification. The values of $C_{p,l}$ and $C_{p,s}$ can be determined by extrapolation from the measured $C_{p,m}$ outside of the temperature range where the solidification takes place.

The temperature dependent enthalpy difference is caused by the difference between the temperature dependent heat capacities of the separate phases:

$$\Delta H_{sl}(T) = H_0 + \int_{T_1}^{T_2} (C_{p,s}(T) - C_{p,l}(T))\mathrm{d}T, \qquad (3)$$

where T_1 is the starting temperature of transformation; T_2 is the temperature where the transformation has just been completed (i.e., $f_s = 1$); H_0, the value of ΔH_{sl} at T_1. The H_0 can be determined according to the following procedure. The starting point of the transformation, where f_l equals 1, is estimated by comparing the measured $C_{p,s}$ curve with the

extrapolated curve for $C_{p,l}$. By prescribing H_0, ΔH_{sl} can be calculated as a function of temperature from T_1 to T_2. These values of ΔH_{sl} are used as inputs to evaluate f_l from the measured $C_{p,s}$. Then the value of H_0 is adjusted in order to satisfy the requirement that the fraction f_s equals 1 at $T = T_2$.

Using the above method, the fraction of solid phase and the determined transformation rate were obtained from the measured apparent heat capacities (Fig. 3). The transformation rate of the solid phase in the investigated alloys, with applied cooling rate of 5 K min^{-1}, was calculated and presented as a function of temperature in Fig. 4.

Several inflection points could be recognized in the obtained curves of the transformation rate. Since the curves reflect the solidification process of the alloys, the inflection points can be recognized as the phase transformation points of them. After comparing with the thermodynamic data and
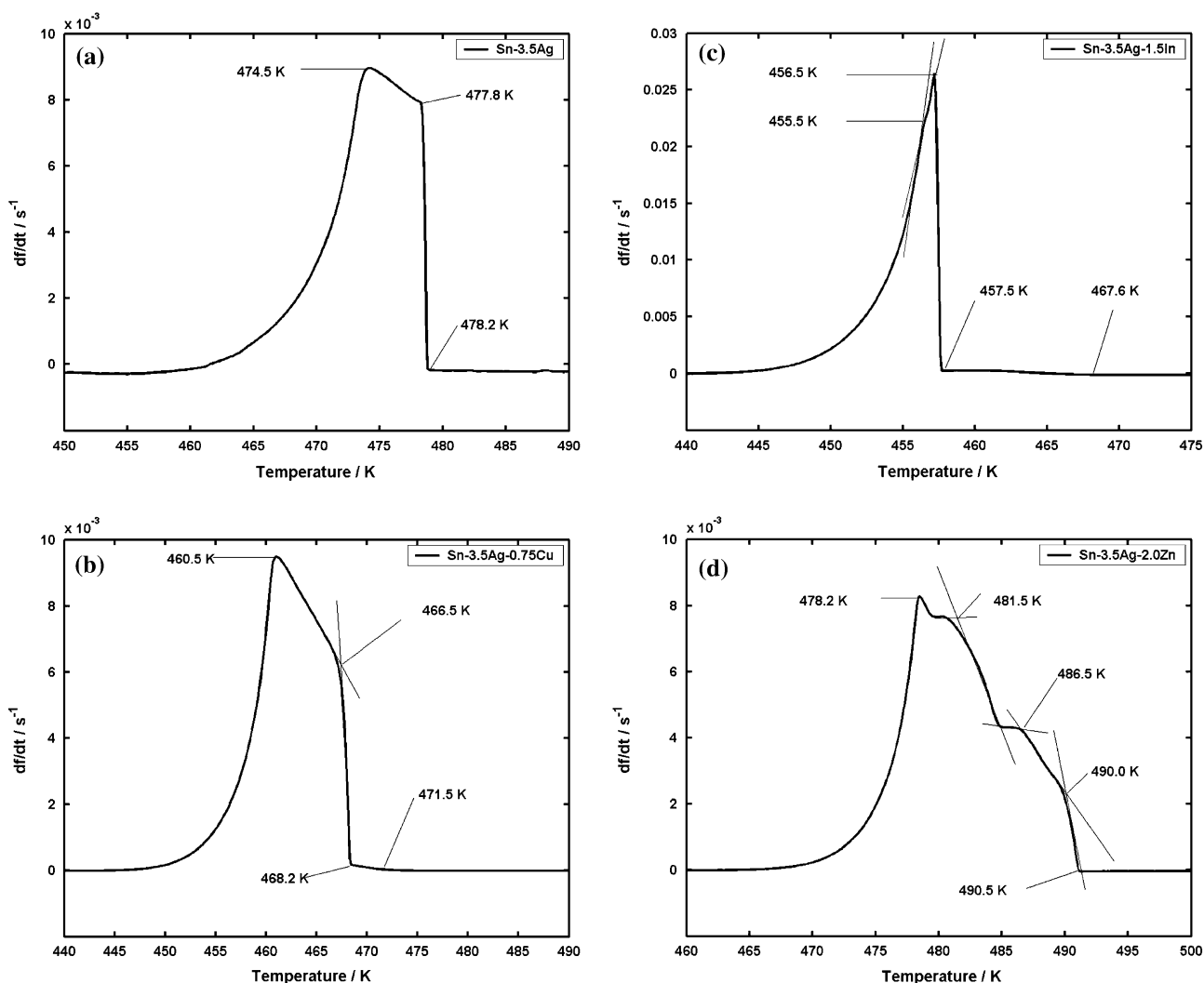

Fig. 4 The relationship between the transformation rate and temperature of alloys as determined from DTA measurements, (**a**) Sn–3.5Ag alloy, (**b**) Sn–3.5Ag–0.75Cu alloy, (**c**) Sn–3.5Ag–1.5In alloy, and (**d**) Sn–3.5Ag–2.0Zn alloy

phase diagram of Sn–Ag [13], Sn–Ag–Cu [14], Sn–Ag–In [15, 16], and Sn–Ag–Zn [17, 18] alloys, it is found that these inflection points are mainly caused by the formation of new phases during alloys solidification. Hence, the corresponding solidification paths of the alloys can be described as:

Sn-3.5Ag alloy: $L \rightarrow L + Ag_3Sn \rightarrow \beta\text{-Sn} + Ag_3Sn$

Sn-3.5Ag-0.75Cu alloy: $L \rightarrow L + Cu_6Sn_5 \rightarrow$

$L + Cu_6Sn_5 + Ag_3Sn \rightarrow \beta\text{-Sn} + Cu_6Sn_5 + Ag_3Sn$

Sn-3.5Ag-1.5In alloy: $L \rightarrow L + Ag_3Sn \rightarrow L + Ag_3Sn$

$+ \beta\text{-Sn} \rightarrow \beta\text{-Sn} + Ag_3Sn + AgIn$

Sn-3.5Ag-2.0Zn alloy: $L \rightarrow L + AgZn \rightarrow$

$L + Ag_5Zn_8 \rightarrow L + AgZn_3 \rightarrow \beta\text{-Sn} + AgZn_3$

There are two phases possessing different growth velocities, and the leading phase is Ag_3Sn during the eutectic reaction in Sn–3.5Ag alloy [19]. Hence, if Ag_3Sn crystal nuclei formed before the onset of eutectic reaction, the leading Ag_3Sn phase could nucleate adjacent to the Ag_3Sn crystal nuclei for their matching crystalline orientation relationships, which would result in the formation of bulk Ag_3Sn IMCs. After comparing with Fig. 4a, it is found that the inflection point (478.2 K) is mainly from the beginning of the bulk Ag_3Sn IMCs formation, the inflection point (477.8 K) is from the end of the bulk Ag_3Sn IMCs formation, and the inflection point (474.5 K) is from the eutectic reaction of Sn–3.5Ag alloy during solidification.

Cu_6Sn_5 phase is the first phase formed in Sn–3.5Ag–0.75Cu alloy during its solidification (from 471.5 K to 468.2 K, see Fig. 4b). Since Cu does not combine with Ag to form any IMCs, bulk Ag_3Sn IMCs formed (from 468.2 to 466.5 K) in this alloy. In Sn–3.5Ag–1.5In alloy, after the formation of Ag_3Sn phase (from 467.6 to 457.5 K), indium combined with Ag to form AgIn phase during it solidification (from 456.5 to 455.5 K, see Fig. 4c). So, indium does not suppress the formation of large Ag_3Sn plates in Sn–3.5Ag–1.5In alloy.

As seen in Fig. 4d, with a minor Zn addition, the solidification of Sn–3.5Ag–2.0Zn alloy experiences two stages of transformation. The first stage is composed of crystallization and double peritectic reactions of the Ag–Zn IMCs at high temperature (from 490.0 to 481.5 K). The second stage is the crystallization of β-Sn at low temperature (at 478.2 K). At the beginning of solidification, the AgZn phase nucleates and grows in the liquid alloy at the expense of nearby Ag and Zn, then it combine with Zn to form Ag_5Zn_8 phase, and then $AgZn_3$ phase. In this process, Ag will be exhausted before it reacted with Sn to form Ag_3Sn phase because of the formation of Ag–Zn IMCs. Hence, a minor Zn addition can suppress the formation of large Ag_3Sn plates in Sn–3.5Ag alloy and the undercooling

degree decrease of Sn–3.5Ag–2.0Zn alloy is attributed to the formation of AgZn phase at high temperature.

5 Conclusions

(1) In the explored slowly cooled lead-free solder alloys, bulk Ag_3Sn IMCs existed in the microstructure of Sn–3.5Ag, Sn–3.5Ag–0.75Cu and Sn–3.5Ag–1.5In alloys, while no bulk Ag_3Sn IMCs formed in Sn–3.5Ag–2.0Zn alloy.

(2) The undercooling degree and solidification process of explored slowly cooled lead-free solder alloys can be easily achieved by the recorded apparent heat capacity curves. The reason for a minor Zn addition suppress the formation of large Ag_3Sn plates in Sn–3.5Ag alloy could be attributed to the preferable reaction of Ag with Zn to form Ag–Zn IMCs at high temperature rather than with Sn.

References

1. M. Abtew, G. Selvaduray, Mater. Sci. Eng. R **27**, 95 (2000)
2. K.S. Kim, S.H. Huh, K. Suganuma, Mater. Sci. Eng. A **333**, 106 (2002)
3. F. Ochoa, J.J. Williams, N. Chawla, JOM **55**, 56 (2003)
4. K.W. Moon, W.J. Boettinger, U.R. Kitten, F.S. Biancaniello, C.A. Handwerker, J. Electron. Mater. **29**, 1122 (2000)
5. I. Ohnuma, M. Miyashita, K. Anzai, X.J. Liu, H. Ohtani, R. Kainuma, K. Ishida, J. Electron. Mater. **29**, 1137 (2000)
6. J. Shen, Y.C. Liu, H.X. Gao, C. Wei, Y.Q. Yang, J. Electron. Mater. **34**, 1591 (2005)
7. J. Shen, Y.C. Liu, Y.J. Han, H.X. Gao, C. Wei, Y.Q. Yang, Trans. Nonferrous Met. Soc. China **16**, 59 (2006)
8. C.M.L. Wu, D.Q. Yu, C.M.T. Law, L. Wang, Mater. Sci. Eng. R **44**, 1 (2004)
9. J. Shen, Y.C. Liu, Y.J. Han, Y.M. Tian, H.X. Gao, J. Electron. Mater. **35**, 1672 (2006)
10. S.K. Kang, D. Leonard, D.Y. Shih, L. Gignac, D.W. Henderson, S. Cho, J. Yu, J. Electron. Mater. **35**, 479 (2006)
11. A.T.W. Kempen, F. Sommer, E.J. Mittemeijer, Thermo. Acta **383**, 21 (2002)
12. A.T.W. Kempen, F. Sommer, E.J. Mittemeijer, Acta Mater. **50**, 3545 (2002)
13. P.Y. Chevalier, Thermo. Acta **136**, 45 (1988)
14. K.S. Kim, S.H. Huh, K. Suganuma, J. Alloy. Compd. **352**, 226 (2003)
15. B. Sundman, B. Jansson, J.O. Andersson, CALPHAD **9**, 153 (1985)
16. W.K. Choi, J.H. Kim, S.W. Jeong, H.M. Lee, J. Mater. Res. **17**, 43 (2002)
17. I. Ohnuma, M. Miyashita, X.J. Liu, H. Ohtani, K. Ishida, IEEE Trans. Electron. Packag. Manuf. **26**, 84 (2003)
18. J.M. Song, K.L. Lina, J. Mater. Res. **19**, 2719 (2004)
19. V. Davies, J. Inst. Metals **10**, 93 (1964)